DOI: 10.1002/chem.200800766

Formation of Diverse Mesophases Templated by a Diprotic Anionic Surfactant

Chuanbo Gao,[a, b] Yasuhiro Sakamoto,[b] Osamu Terasaki,[b] and Shunai Che*[a]

Abstract: The synthesis system for mesophase formation, using the diprotic anionic surfactant *N*-myristoyl-L-glutamic acid (C_{14}GluA) as the structure-directing agent (SDA) and *N*-trimethoxylsilylpropyl-*N,N,N*-trimethylammonium chloride (TMAPS) as the co-structure-directing agent (CSDA), has been investigated and a full-scaled synthesis-field diagram is presented. In this system we have obtained mesophases including three-dimensional (3D) micellar cubic $Fm\bar{3}m$, $Pm\bar{3}n$, $Fd\bar{3}m$, micellar tetragonal $P4_2/mnm$, two-dimensional (2D) hexagonal *p6mm* and bicontinuous cubic $Pn\bar{3}m$, by varying the C_{14}GluA/NaOH/TMAPS composition ratios. From the diagram it can be concluded that the mesophase formation is affected to a high degree by the organic/inorganic-interface curvature and the mesocage–mesocage electrostatic interaction. Bicontinuous cubic and 2D-hexagonal phases were found in the low organic/inorganic-interface curvature zones, whereas micellar cubic and tetragonal mesophases were found in the high organic/inorganic-interface curvature zones. Formation of cubic $Fm\bar{3}m$ and tetragonal $P4_2/mnm$ was favoured in highly alkaline zones with strong mesocage–mesocage interactions, and formation of cubic $Pm\bar{3}n$ and $Fd\bar{3}m$ was favoured with moderate mesocage–mesocage interactions in the less alkaline zones of the diagram.

Keywords: formation mechanism · mesophases · mesoporous materials · surfactants · synthesis-field diagram

Introduction

Since the discovery of mesoporous silica in the last decade,[1,2] various mesophases have been found and resolved including the cage-type tetragonal ($P4_2/mnm$,[3] etc.), 3D hexagonal ($P6_3/mmc$[4]), cubic ($Pm\bar{3}n$,[5,6] $Fd\bar{3}m$,[7,8] $Im\bar{3}m$,[6,9] $Fm\bar{3}m$,[10,11] etc), bicontinuous cubic ($Ia\bar{3}d$,[2,12] $Pn\bar{3}m$,[13] etc), 2D hexagonal (*p6mm*[2,14]), and lamellar phase.[2] The mesoporous silicas that have these mesostructures were obtained from different synthesis systems by using cationic, anionic or non-ionic surfactants as a structure-directing agent (SDA). Because of the complexity of the synthesis systems it is difficult to find the formation mechanisms of these mesophases, even though a simplified surfactant packing parameter *g*[15] was employed to predict the mesophase.[16]

Anionic-surfactant templating method, first reported by Che et al.,[17] affords diverse mesoporous silicas with high crystallinity, including anionic-surfactant templated mesoporous silica (AMS), (AMS)-1~10,[17–20,3,13] and a chiral mesoporous silica with helical morphology.[21–23] Therefore, this system is a good candidate for the investigation of the formation mechanisms and the relationships of different mesophases. Moreover, these kinds of mesoporous material are homogeneously functionalised with organic moieties, and have a high loading efficiency through the interactions between surfactant headgroups and the amino or quaternary ammonium groups of a co-structure-directing agent (CSDA). Therefore, AMS has attracted much attention of the researchers with different scientific interests including material science, structural physics, supermolecular chemistry and pharmacy.

The capacity of the AMS synthesis system to form diverse and highly-ordered mesophases can be mainly attributed to the introduction of an additional co-structure-directing effect by the inclusion of aminopropylsiloxane or quaternised aminopropylsiloxane in the inorganic precursors to act as a CSDA. The negatively charged headgroups of the

[a] C. Gao, Prof. S. Che
School of Chemistry and Chemical Technology
State Key Laboratory of Composite Materials
Shanghai Jiao Tong University, Shanghai 200240 (China)
Fax: (+86) 21-5474-1297
E-mail: chesa@sjtu.edu.cn

[b] C. Gao, Dr. Y. Sakamoto, Prof. O. Terasaki
Structural Chemistry
Arrhenius Laboratory
Stockholm University, 10691 Stockholm (Sweden)

Supporting information for this article is available on the WWW under http://dx.doi.org/10.1002/chem.200800766.

anionic surfactants interact electrostatically with the positively charged ammonium sites of the CSDAs, while the alkoxysilane groups of the CSDA co-condense with tetraalkoxysilane and are subsequently assembled to form the silica framework.[17] The interaction between the wall-forming precursors and the surfactant by this method is much stronger than that in the conventional synthesis of mesoporous silicas, examples including MCM-41 and SBA-15.[2,14] This strong organic/inorganic electrostatic interaction serves as the driving force of the formation of highly ordered AMS mesostructures.

It is also found that well-ordered mesophases in decreasing order of organic/inorganic-interface curvature from cage-type (tetragonal $P4_2/mnm$; cubic $Pm\bar{3}n$ with modulations and cubic $Fd\bar{3}m$), to 2D hexagonal ($p6mm$), bicontinuous cubic ($Ia\bar{3}d$ and $Pn\bar{3}m$) and lamellar, can be easily controlled by decreasing the ionization degree of the weakly acidic anionic surfactant.[19] It has been considered that a decrease in the degree of ionization of the surfactant leads to a reduction in the negative-charge density on the micelles, which further results in a decrease in the electrostatic repulsion of the surfactant headgroups and the headgroup area in micelles. The smaller headgroup area leads to a larger surfactant-packing parameter, g, which gives rise to mesophases with smaller organic/inorganic interface curvatures. Moreover, it is also reported that by controlling the reaction kinetics, different cage-type mesostructures including $P4_2/mnm$, $Pm\bar{3}n$, $Fd\bar{3}m$ and a modulated structure can be obtained.[3] Nevertheless, the precise mechanism of the mesophase determination is not well understood.

Herein we present a full-scaled synthesis-field diagram of the mesoporous silicas prepared with diprotic anionic surfactant *N*-myristoyl-L-glutamic acid (C_{14}GluA) as the SDA and *N*-trimethoxylsilylpropyl-*N,N,N*-trimethylammonium chloride (TMAPS) as the CSDA. We chose diprotic C_{14}GluA as the referenced SDA, because it has two carboxylate groups, which creates the possibility of forming different mesophases with highly curved organic/inorganic interface curvatures as well as mesophases with reduced curvature. Water soluble TMAPS, which has a permanent positive charge, interacts with anionic surfactant in an electrostatic way and serves as the counterion of the anionic surfactant. The amount of tetraethyl orthosilicate (TEOS) in the synthesis of AMS within a certain range does not have significant effects on the curvature of the resultant mesophase. Therefore, the key factors of the mesophase formation has been determined as SDA C_{14}GluA, CSDA TMAPS, and NaOH, the compositions of which have been changed, while keeping other factors (the concentration of surfactant, the TEOS/C_{14}GluA ratio and temperature) constant to get the full picture of the diagram. On the basis of the synthesis-field diagram the formation mechanism and the structural relationship of different mesophases have been further discussed in details.

Results and Discussion

Diverse mesostructures in the synthesis-field diagram: Sixty-four compositions were carefully chosen to complete the synthesis-field diagram of the C_{14}GluA/NaOH/TMAPS synthesis system (Figure 1). The determination of the mesostructure was on the basis of X-ray diffraction (XRD) patterns and HRTEM images. The synthesis conditions of the mesophases are summarised in Table 1.

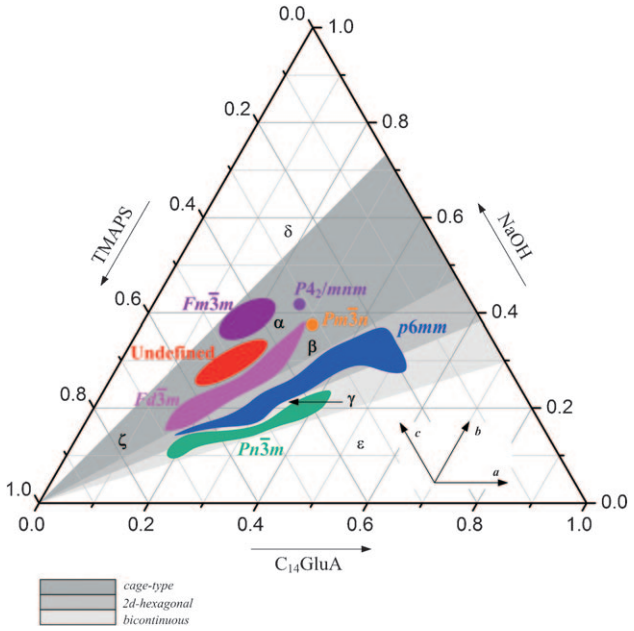

Figure 1. Synthesis-field diagram (mole fraction) of the C_{14}GluA/NaOH/TMAPS synthesis system.

Table 1. Synthesis conditions of the mesophases in the C_{14}GluA/NaOH/TMAPS system.

Mesophase	Mesopore type	pH[a]	NaOH/ C_{14}GluA	TMAPS/ C_{14}GluA
$Pn\bar{3}m$	bicontinuous	5.0–5.2	0.45–0.62	0.84–3.8
$p6mm$	cylindrical	5.2–5.6	0.62–0.86	0.35–3.8
$Fd\bar{3}m$	micellar cubic	5.6–6.2	0.86–1.25	1.1–4.5
undefined	–	6.2–7.4	1.25–1.7	1.6–3.8
$Pm\bar{3}n$	micellar cubic	6.1	1.16	1.0
$P4_2/mnm$	micellar tetragonal	6.7	1.56	1.2
$Fm\bar{3}m$	micellar cubic	7.4–11.0	1.7–2.7	1.6–3.3

[a] The pH of the reaction solution was measured at 70 °C before the addition of TMAPS and TEOS.

The XRD pattern of the mesoporous silica synthesised with the space group of $Pn\bar{3}m$ (Supporting Information, Figure S1), as the composition shown in Figure 1, has two well-resolved peaks with the reciprocal d-spacing ratio of $\sqrt{2}/\sqrt{3}$, which can be assigned to 110 and 111 reflections. According to the analysis of its high-resolution transmission electron microscopy (HRTEM, images not shown), the mesostructure is confirmed to be bicontinuous cubic $Pn\bar{3}m$, composed

of an enantiomeric pair of 3D-mesoporous networks that are interwoven with each other.[13] The three peaks of the typical XRD pattern of the mesoporous silica with the 2D-hexagonal symmetry (Supporting Information, Figure S1) can be well assigned to 10, 11, and 20 reflections of the *p6mm* space group. These two structures, bicontinuous $Pn\bar{3}m$ and *p6mm*, which show a low organic/inorganic-interface curvature and the bicontinuous/cylindrical mesopore geometry, were formed within a pH range of as low as 5.0–5.6 and NaOH/C_{14}GluA ratio of 0.45–0.86 (Table 1).

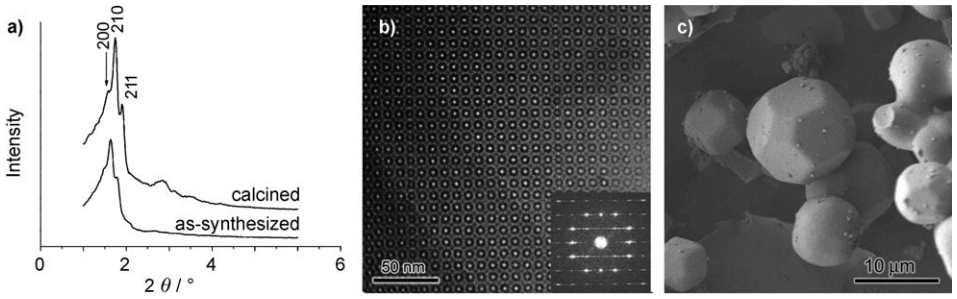

Figure 2. a) XRD pattern, b) HRTEM image, and c) SEM image of the cage-type mesoporous silica that has the space group cubic $Pm\bar{3}n$: C_{14}GluA/NaOH/TMAPS 0.317:0.367:0.317.

The cage-type mesophases, including cubic $Fd\bar{3}m$, cubic $Pm\bar{3}n$, tetragonal $P4_2/mnm$ and cubic $Fm\bar{3}m$, have been prepared by changing the C_{14}GluA/NaOH/TMAPS compositions. These mesophases are formed in the systems with a high ionization degree of surfactant (NaOH/C_{14}GluA = 0.86–2.7) showing a relatively high pH of 5.6–11.0. The occurrence of each mesophase in the synthesis-field diagram has been described in Figure 1 and Table 1.

The typical XRD pattern, HRTEM and scanning electron microscopy (SEM) images of the cubic $Fd\bar{3}m$ mesophase are shown in the Supporting Information (Figure S2). The HRTEM image taken along [110] direction clearly reveals the mesostructure, and the two well-resolved peaks in the 1–6 ° 2θ of the XRD pattern with a $\sqrt{2}/\sqrt{3}$ reciprocal *d*-spacing ratio can be indexed to 220 and 222 reflections of the $Fd\bar{3}m$ space group. An existence of twin planes, which can be clearly observed in the HRTEM image, produces streaks in the Fourier diffractogram inserted in the image. The morphology of the sample observed from the SEM is crystal-like and is typically cubic having $m\bar{3}m$ symmetry. This mesophase was formed within a TMAPS/C_{14}GluA range of 1.1–4.5 and a NaOH/C_{14}GluA range of 0.86–1.25 showing a pH of 5.6–6.2.

The typical XRD pattern, HRTEM, and SEM images of the cubic $Pm\bar{3}n$ mesophase are shown in Figure 2. The XRD pattern showing three diffraction peaks with a reciprocal *d*-spacing ratio of $\sqrt{4}/\sqrt{5}/\sqrt{6}$ can be well indexed as the 200, 210, and 211 reflections, consistent with the $Pm\bar{3}n$ space group. The HRTEM images taken along [100] zone axis and the dodecahedron crystal morphology demonstrated by the SEM image strongly confirm the mesostructure. It shows $m\bar{3}m$ point group symmetry. In the HRTEM image we can observe planar defects, which give rise to diffuse scattering in the Fourier diffractogram. The mesostructure was formed with a NaOH/C_{14}GluA ratio of 1.16 showing a pH of 6.1, and the TMAPS content in the system was lower (TMAPS/C_{14}GluA = 1.0) than that of the $Fd\bar{3}m$ synthesis system.

The typical XRD pattern, HRTEM image, and SEM image of the mesophase $P4_2/mnm$ are collected in the Supporting Information (Figure S3). The XRD pattern is difficult to index, because no detailed peaks are presented within the range of 1–6° 2θ. However, from the HRTEM image taken along [001] zone axis, the mesostructure can be determined as tetragonal $P4_2/mnm$. The SEM image shows that the sample possesses tetragonal morphology and has 4/*mmm* point group symmetry, which confirms the tetragonal mesostructure. The structure shows many X-ray reflections, which makes the XRD pattern hard to index. The tetragonal mesophase was formed at a TMAPS/C_{14}GluA ratio of 1.2 and a NaOH/C_{14}GluA ratio of 1.56 showing a pH of 6.7.

The typical XRD pattern, HRTEM, and SEM images of the face-cantered cubic $Fm\bar{3}m$ mesostructure is shown in Figure 3. The XRD peaks can be indexed to 111, 200, 220, and 311 reflections, indicating a high crystallinity. The HRTEM image taken in [110] direction clearly confirms the mesostructure. Figure 3c shows a polyhedron crystal of the structure, which does not fit $m\bar{3}m$ point group symmetry. This morphology can be explained by twinning commonly observed in face cantered cubic $Fm\bar{3}m$ structure.[24] This mesophase was formed at a high pH of 7.4–11.0 with a TMAPS/C_{14}GluA ratio of 1.6–3.3 and a NaOH/C_{14}GluA ratio of 1.7–2.7.

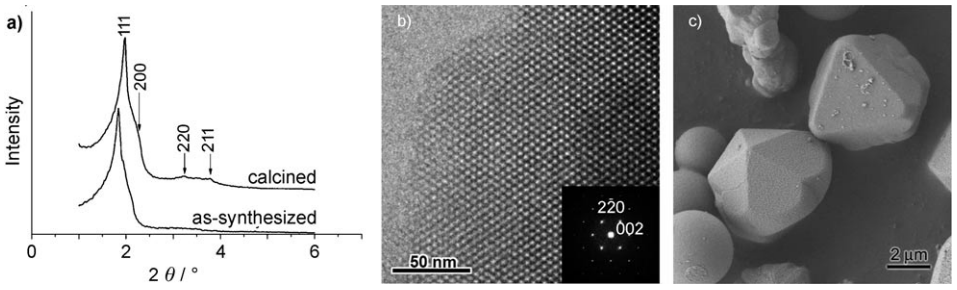

Figure 3. a) XRD pattern, b) HRTEM image, and c) SEM image of the cage-type mesoporous silica that has the space group cubic $Fm\bar{3}m$: C_{14}GluA/NaOH/TMAPS 0.200:0.400:0.400.

A zone around C_{14}GluA/NaOH/TMAPS 0.2:0.3:0.5 in the diagram gives rise to a undefined cage-type mesophase, which was formed at a pH of 6.2–7.4. The hydrolysis of TMAPS and silica source TEOS was very low within this range of pH, which hindered the self-organization of the organic/inorganic species and the formation of stable ordered mesophases. The mesophase formed is unstable and easily collapses during the thermal treatment at 550 °C. The structure is not fully understood and is under further investigation. (see the HRTEM images in Figure S4 of the Supporting Information)

Notably, in Figure 1, composition points in zone α gives rise to a coexistence of *Fd*$\bar{3}$*m*, *Pm*$\bar{3}$*n*, $P4_2/mnm$, and *Fm*$\bar{3}$*m* (Supporting Information, Figure S5); composition points in zone β give a mixture of cubic and 2D-hexagonal phase (Supporting Information, Figure S6); and a mixed phase comprising bicontinuous cubic *Pn*$\bar{3}$*m* and 2D hexagonal *p6mm* could be found in zone γ (Supporting Information, Figure S7). However, in the zones δ, ε, or ζ, mesoporous silicas could not be formed because the mole fraction of NaOH, C_{14}GluA or TMAPS, respectively, was too high.

The diverse mesophases, as have been described above, were achieved in the same synthesis system but different composition ratios. It proved the versatility of the mesophase formation by using the diprotic anionic surfactant C_nGluA as the SDA by means of the co-structure-directing method. On the other hand, the diverse mesophases formed in the same system make it possible for the study on the structure occurrence, dependence, and formation mechanism.

Effect of the synthesis composition on the mesostructure: From the diagram shown in Figure 1, it can be inferred that the phase fields are strip-like, lie in the sector zones, and employ C_{14}GluA/NaOH/TMAPS 0:0:1 as the vertex (as the shadow zones in Figure 1 shows). It is known that when changing the composition point down a line, starting at the point C_{14}GluA/NaOH/TMAPS 0:0:1 in the synthesis-field diagram, the ratio of NaOH/C_{14}GluA is kept constant and the ratios of TMAPS/NaOH and TMAPS/C_{14}GluA are decreasing. Therefore, the strip-like distribution of the mesophases in the diagram indicates that the determining factor of the mesophase formation is the ionization degree of the surfactant (NaOH/C_{14}GluA); the effect of the amount of TMAPS in the synthesis gel on the mesophase formation is not prominent. The change in the fraction of TMAPS in the synthesis gel could not dramatically change the mesophase obtained, especially in the zones of bicontinuous cubic and 2D hexagonal. Notably, the mesophase changes could be also observed in the zones of the cage-type mesophase from tetragonal $P4_2/mnm$ to an undefined cage-type phase and from cubic *Pm*$\bar{3}$*n* to cubic *Fd*$\bar{3}$*m*, as a result of an increase of the mole fraction of TMAPS in the C_{14}GluA/TMAPS/NaOH tri-component system.

When keeping the mole fraction of TMAPS constant in the C_{14}GluA/TMAPS/NaOH system and increasing the NaOH/C_{14}GluA ratio, the composition point changes down a line in direction *c* in the diagram, and the structure of the mesoporous silica obtained changes from bicontinuous cubic *Pn*$\bar{3}$*m* to 2D hexagonal *p6mm*, cubic *Fd*$\bar{3}$*m*, an undefined cage-type phase, and cubic *Fm*$\bar{3}$*m*; from 2D hexagonal *p6mm* to cubic *Pm*$\bar{3}$*n* and tetragonal $P4_2/mnm$. These changes of mesophases show a dramatic mesopore geometry change from bicontinuous to cylindrical and further cage-types, with an increase of the organic/inorganic interface curvature.

Mesophase formation dominated by the organic/inorganic interface curvature: As a conclusion of the above discussions, the bicontinuous cubic phase, which has a low organic/inorganic-interface curvature ($1/2 < g < 1$), has been obtained in the zones with low surfactant ionization degree (NaOH/C_{14}GluA = 0.45–0.62) showing an initial pH of 5.0–5.2. The 2D-hexagonal phase, whose organic/inorganic-interface curvature ($g = 1/2$) is larger than bicontinuous cubic, was synthesised in the zones with a moderate ionization degree of surfactant (NaOH/C_{14}GluA = 0.62–0.86), with an initial pH of 5.2–5.6. Increasing the ratio of NaOH/C_{14}GluA to 0.86–2.7, or increasing the pH of synthesis system to 5.6–11.0 lead to the formation of cage-type mesophases with the largest organic/inorganic-interface curvature ($g = 1/3$).

In our earlier works[13,19] we have described that in the synthesis of AMS, higher alkalinity favours the formation of mesophases with high organic/inorganic-interface curvature, owing to the lager ionization degree of the anionic surfactant. From the full-scaled synthesis-field diagram shown in Figure 1, this change of mesophase from bicontinuous cubic to 2D hexagonal and further cage-type, triggered by the increase of the ionization degree of the surfactant, proves the dominating rule of the organic/inorganic-interface curvature on the mesophase determination.

Mesophase formation affected by the mesocage–mesocage electrostatic interactions: The organic/inorganic-interface curvature dominates the change of mesophase from bicontinuous cubic to 2D hexagonal and further cage-type; however, it cannot explain the packing manner of the mesocages in the cage-type zone and the formation mechanism of different 3D mesostructures, which has been long pursued by scientists. Our system affords various cage-type mesostructures by simply varying the mole fraction, which provides experimental foundations to propose a possible formation mechanism as described in Scheme 1.

In the formation of cage-type mesostructures anionic surfactant molecules form micelles to reduce the free energy, which makes a negatively charged surface. On the outside of this surface, to balance the negative charge, positively charged CSDA distributes in both the Stern layer in which immobile CSDA cations are tightly bonded to the surface and the diffuse layer in which mobile CSDA cations weakly interact with the charged surface (Scheme 1). The micelles and the inorganic species in the Stern layer, which together are defined as a "mesocage", are then packed by certain means with the hydrolyzed TEOS to form the mesostruc-

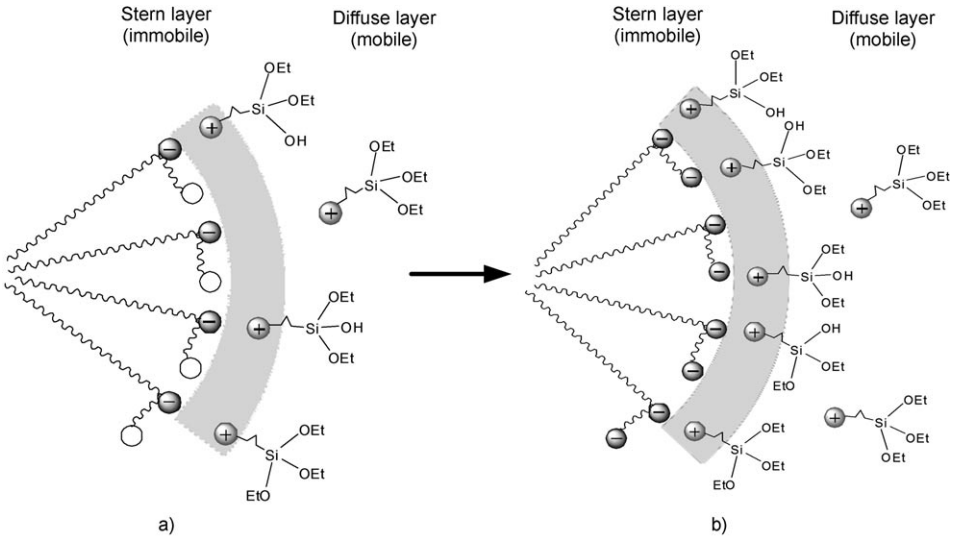

Scheme 1. Different charging states of mesocage: a) The mesocage is mildly negatively charged when the surfactant micelle shows low-charge density; b) The mesocage is highly negatively charged when the micelle shows high-charge density. The different charging state leads to different interactions between the mesocages and different packing manners.

ture. In this model, the "mesocage" acts as a "brick" and the hydrolyzed TEOS acts as "mortar", and the interactions between the "bricks" dominate the structure of the formed composite matrix.

These building blocks of the cage-type mesostructures, mesocages, are negatively charged, because the positive charges in the Stern layer could not balance the negative charges of the micelles, which could only be achieved at an infinite distance. The electrostatic interaction between the mesocages changes with the charging state of the micelles and further determines the packing manner of these mesocages. As described in Scheme 1, qualitatively speaking, when the charge density of the micelles is low, the mesocages are mildly charged, and the mesocage–mesocage electrostatic interaction is weak; on the contrary, when the charge density of the micelles gets higher, the mesocages are highly charged, and the mesocage–mesocage electrostatic interaction gets strong.

From our results shown in Figure 1 and Table 1 it can be inferred that, in the mildly alkaline zones of the diagram (the initial pH of the C_{14}GluA solution is 5.6–6.2), the ionization degree of surfactant is relatively low (NaOH/C_{14}GluA = 0.86–1.25), and therefore the mesocages are moderately charged and the interactions are relatively weak; cubic $Pm\bar{3}n$ and $Fd\bar{3}m$ were formed when packing of these mesocages. If the ionization degree of the surfactant gets higher (NaOH/C_{14}GluA = 1.56) at more alkaline conditions (the initial pH of the C_{14}GluA solution is 6.7), the mesocages are highly charged because of the high charge density on the micelle surfaces, and therefore the mesocage–mesocage interactions are strong; tetragonal $P4_2/mnm$ can be found in these zones of the diagram. If the reaction is carried out under even stronger alkaline conditions (the initial pH is 7.4–11.0), the strong mesocage–mesocage interactions, caused by the highly charged mesocages, give rise to a face-centered close-packed cubic $Fm\bar{3}m$ mesophase. It can be inferred that the charging state of the mesocages or the mesocage–mesocage interactions is the determining factor of the packing of the mesocages and formation of cage-type mesostructures.

It can be also inferred from the results that cubic $Pm\bar{3}n$ and tetragonal $P4_2/mnm$ were formed in the synthesis system with low mole fraction of TMAPS (TMAPS/C_{14}GluA = 1.0 and 1.2, respectively), and cubic $Fd\bar{3}m$ and $Fm\bar{3}m$ were formed with a high content of TMAPS in the system (TMAPS/C_{14}GluA = 1.1–4.5 and 1.6–3.3, respectively). It indicates that the mole fraction of CSDA also affects the structure of the mesoporous silica to an extent, which may be attributed to the screening of the mesocage–mesocage electrostatic repulsion by the diffused CSDA cations in the synthesis system.

The packing of charged identical hard spheres has been investigated and the particle volume fraction, particle charging and dipoles have been considered the factors of the hard sphere packing.[25] To a great extent the hard sphere packing system is similar to the synthesis system of mesoporous silica and the results are fairly consistent. However, in our system, because of the soft nature of the synthesis approach and the need to minimise the free energy and occupy the space, the system itself would adopt a more versatile strategy and more abundant phases could be obtained, for example, $Pm\bar{3}n$, $Fd\bar{3}m$ and $P4_2/mnm$, in which there are at least two types of micelles with different sizes and shapes.[6,8]

Furthermore, from the perspective of the mesocage–mesocage interaction we can propose a reasonable mechanism of the mesophase change through varying the delayed time (t) of the addition of TEOS after 3-aminopropyltriethoxylsilane (APES) reported by Garcia-Bennett et al.[3] It is known that the rate of hydrolysis and condensation of organotriethylsilane is lower than TEOS, and a larger value of the delayed time t makes a pre-hydrolyzed APES and thus facilitates the co-condensation of APES and TEOS. It leads to a Stern layer with lower positive charge density and therefore larger mesocage–mesocage interactions. However, the further elongation of the time t results in a self-condensation of APES, which leads to a higher positive charge density of the Stern layer and therefore lower mesocage–mesocage interactions. As a result, mesophase changes from $Fd\bar{3}m$ to $P4_2/mnm$, and further from $P4_2/mnm$ to $Pm\bar{3}n$ and $Fd\bar{3}m$ were observed by delaying the addition of TEOS.

Conclusion

The formation of the mesophases in the C_{14}GluA/NaOH/TMAPS synthesis system of AMS was discussed in detail, and the full-scaled synthesis-field diagram was presented. This synthesis system can form diverse mesophases, which include cubic $Fm\bar{3}m$, $Pm\bar{3}n$, $Fd\bar{3}m$, $Pn\bar{3}m$, tetragonal $P4_2/mnm$, and 2D hexagonal $p6mm$. According to the occurrence of each of the mesophase, it can be inferred that the mesophase formation is affected by both the organic/inorganic-interface curvature and the mesocage–mesocage interactions. The organic/inorganic-interface curvature determines if the mesopore geometry is layered, bicontinuous, cylindrical, or cage-type. Lower charging of the mesocage, and therefore weaker mesocage–mesocage interactions, results in a mesocage packing manner of cubic $Pm\bar{3}n$ or $Fd\bar{3}m$, tetragonal $P4_2/mnm$, and cubic $Fm\bar{3}m$ were formed in the highly alkaline zones with strong mesocage–mesocage interactions. These findings may be useful in the mesophase design and control of not only the AMS materials, but also the cationic and nonionic surfactant templated mesoporous silicas. It could also provide certain information to the researchers in the fields of liquid crystals and structural analysis.

Experimental Section

Synthesis of diprotic anionic surfactant C_{14}GluA: Anionic surfactant *N*-myristoyl-L-glutamic acid C_{14}GluA was synthesised by a previously reported method.[13] To a solution prepared from L-glutamic acid (35.5 g, 0.24 mol) in water (140 mL), acetone (120 mL), and sodium hydroxide (19.2 g) myristoyl chloride (49.3 g, 0.2 mol), and sodium hydroxide (8.0 g, 0.2 mol) in water (20 mL) were added with stirring at 0 °C and at pH 12 over a period of 20 min. The reaction mixture was stirred for one additional hour, and acidified to pH 1 with sulfuric acid. Crude crystals of C_{14}GluA precipitated, were washed in petroleum ether, and deionised water to obtain the pure crystals, which were then dried in vacuum.

Synthesis of mesoporous materials: When preparing the C_{14}GluA/NaOH/TMAPS triangle synthesis-field diagram, each of the three chemical components has been changed in the synthesis, keeping the following conditions constant: concentration of the surfactant in water = 1 wt %; TEOS/surfactant = 15; synthesis temperature: 70 °C.

Typical synthesis of mesoporous silica (mesostructure: $Pm\bar{3}n$): C_{14}GluA (0.357 g, 1 mmol) was first dispersed in deionised water at 70 °C. To the solution, 1 M NaOH (1.16 g) was added with stirring. A mixture of TEOS (3.12 g, 15 mmol) and TMAPS (0.515 g, 1 mmol, 50 wt % in methanol) was added with stirring. After 10 minutes the stirring was stopped and the reaction mixture was aged at 70 °C for 2 days. The precipitate was filtered, dried at 50 °C, and calcined at 550 °C for 6 h to give surfactant-free mesoporous silica.

Characterizations: Powder X-ray diffraction (XRD) patterns were recorded by using a Rigaku X-ray diffractometer D/MAX-2200/PC equipped with $Cu_{K\alpha}$ radiation (40 kV, 20 mA) at the rate of 1.0°/min over the range of 1–6° (2θ). High-resolution transmission electron microscopy (HRTEM) was performed by using a JEOL JEM-3010 microscope operating at 300 kV ($Cs = 0.6\,mm$, resolution 1.7 Å). Images were recorded by means of a CCD camera (MultiScan model 794, Gatan, 1024 × 1024 pixels, pixel size 24 × 24 μm) at 50–80 k magnification under low-dose conditions. The microscopic morphological features were observed by using a SEM (JEOLJSM-7401F). An accelerating voltage, 1 kV (resolution: ≈1.4 nm) was chosen for all mesoporous silica samples.

Acknowledgements

This work was supported by National Natural Science Foundation of China (Grant No. 20425102 and 20521140450) and the China Ministry of Education. OT and YS thank Swedish Research Council (VR) and Japan Science and Technology Agency (JST) for financial support.

[1] T. Yanagisawa, T. Shimizu, K. Kuroda, C. Kato, *Bull. Chem. Soc. Jpn.* **1990**, *63*, 988–992.
[2] J. S. Beck, J. C. VartUli, W. J. Roth, M. E. Leonowicz, C. T. Kresge, K. D. Schmitt, C. T-W. Chu, D. H. Olson, E. W. Sheppard, S. B. McCullen, J. B. Higgins, J. L. Schlenkert, *J. Am. Chem. Soc.* **1992**, *114*, 10834–10843.
[3] A. E. Garcia-Bennett, N. Kupferschmidt, Y. Sakamoto, S. Che, O. Terasaki, *Angew. Chem.* **2005**, *117*, 5451–5456; *Angew. Chem. Int. Ed.* **2005**, *44*, 5317–5322.
[4] Q. Huo, R. Leon, P. M. Petroff, G. D. Stucky, *Science* **1995**, *268*, 1324–1327.
[5] Q. Huo, D. I. Margolese, U. Ciesla, P. Feng, T. E. Gier, P. Sieger, R. Leon, G. D. Stucky, *Nature* **1994**, *368*, 317–321.
[6] Y. Sakamoto, M. Kaneda, O. Terasaki, D. Zhao, J. M. Kim, G. D. Stucky, H. J. Shin, R. Ryoo, *Nature* **2000**, *408*, 449–453.
[7] S. Shen, Y. Li, Z. Zhang, J. Fan, B. Tu, W. Zhou, D. Zhao, *Chem. Commun.* **2002**, 2212–2213.
[8] A. E. Garcia-Bennett, K. Miyasaka, O. Terasaki, S. Che, *Chem. Mater.* **2004**, *16*, 3597–3605.
[9] D. Zhao, Q. Huo, J. Feng, B. F. Chmelka, G. D. Stucky, *J. Am. Chem. Soc.* **1998**, *120*, 6024–6036.
[10] J. Fan, C. Yu, F. Gao, J. Lei, B. Tian, L. Wang, Q. Luo, B. Tu, W. Zhou, D. Zhao, *Angew. Chem.* **2003**, *115*, 3254–3258; *Angew. Chem. Int. Ed.* **2003**, *42*, 3146–3150.
[11] Y. Sakamoto, I. Díaz, O. Terasaki, D. Zhao, J. Pérez-Pariente, J. M. Kim, G. D. Stucky, *J. Phys. Chem. B* **2002**, *106*, 3118–3123.
[12] A. Carlsson, M. Kaneda, Y. Sakamoto, O. Terasaki, R. Ryoo, S. H. Joo, *J. Electron Microsc.* **1999**, *48*, 795–798.
[13] C. Gao, Y. Sakamoto, K. Sakamoto, O. Terasaki, S. Che, *Angew. Chem.* **2006**, *118*, 4401–4404; *Angew. Chem. Int. Ed.* **2006**, *45*, 4295–4298.
[14] D. Zhao, J. Feng, Q. Huo, N. Melosh, G. H. Fredrickson, B. F. Chmelka, G. D. Stucky, *Science* **1998**, *279*, 548–552.
[15] J. N. Israelachvili, D. J. Mitchell, B. W. Ninham, *J. Chem. Soc. Faraday Trans. 2.* **1976**, *72*, 1525–1568.
[16] Q. Huo, D. I. Margolese, G. D. Stucky, *Chem. Mater.* **1996**, *8*, 1147–1160.
[17] S. Che, A. E. Garcia-Bennett, T. Yokoi, K. Sakamoto, H. Kunieda, O. Terasaki, T. Tatsumi, *Nature Mater.* **2003**, *2*, 801–805.
[18] A. E. Garcia-Bennett, O. Terasaki, S. Che, T. Tatsumi, *Chem. Mater.* **2004**, *16*, 813–821.
[19] C. Gao, H. Qiu, W. Zeng, Y. Sakamoto, O. Terasaki, K. Sakamoto, C. Chen, S. Che, *Chem. Mater.* **2006**, *18*, 3904–3914.
[20] C. Gao. Y. Sakamoto, O. Terasaki, K. Sakamoto, S. Che, *J. Mater. Chem.* **2007**, *17*, 3591–3602.
[21] S. Che, Z. Liu, T. Ohsuna, K. Sakamoto, O. Terasaki, T. Tatsumi, *Nature* **2004**, *429*, 281–284.
[22] H. Jin, Z. Liu, T. Ohsuna, O. Terasaki, Y. Inoue, K. Sakamoto, T. Nakanishi, K. Ariga, S. Che, *Adv. Mater.* **2006**, *18*, 593–596.
[23] X. Wu, H. Jin, Z. Liu, T. Ohsuna, O. Terasaki, K. Sakamoto, S. Che, *Chem. Mater.* **2006**, *18*, 241–243.
[24] K. Miyasaka, L. Han, S. Che, O. Terasaki, *Angew. Chem.* **2006**, *118*, 6666–6669; *Angew. Chem. Int. Ed.* **2006**, *45*, 6516–6519.
[25] A. Yethiraj, A. van Blaaderen, *Nature*, **2003**, *421*, 513–517.

Received: April 22, 2008
Published online: November 14, 2008

